AD-A052 268 AIR FORCE GEOPHYSICS LAB HANSCOM AFB MASS F/G 4/1
LARGE AMPLITUDE IRREGULARITIES AT LOW LATITUDES IN THE TOPSIDE --ETC(U)
NOV 77 W J BURKE, D E DONATELLI, R C SAGALYN

UNCLASSIFIED AFGL-TR-77-0263 NL

| OF |
AD
A052 268

END
DATE
FILMED
5-78
DDC

AFGL-TR-77-0263
ENVIRONMENTAL RESEARCH PAPERS, NO. 616

(2)

B.S.

Large Amplitude Irregularities at Low Latitudes in the Topside Ionosphere

W. J. BURKE
D. E. DONATELLI
R. C. SAGALYN
M. C. KELLEY

28 November 1977

SPACE PHYSICS DIVISION PROJECT 2311
AIR FORCE GEOPHYSICS LABORATORY
HANSCOM AFB, MASSACHUSETTS 01731

AIR FORCE SYSTEMS COMMAND, USAF

This report has been reviewed by the ESD Information Office (OI) and is releasable to the National Technical Information Service (NTIS).

This technical report has been reviewed and is approved for publication.

FOR THE COMMANDER

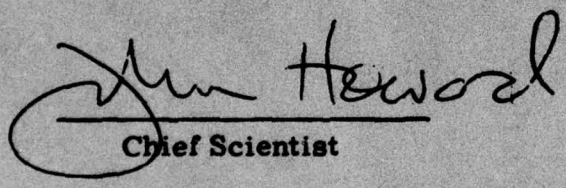

Chief Scientist

Qualified requestors may obtain additional copies from the Defense Documentation Center. All others should apply to the National Technical Information Service.

(9) Environmental research papers,

Unclassified
SECURITY CLASSIFICATION OF THIS PAGE (When Data Entered)

REPORT DOCUMENTATION PAGE	READ INSTRUCTIONS BEFORE COMPLETING FORM
1. REPORT NUMBER: (14) AFGL-TR-77-0263, AFGL-ERP-616	3. RECIPIENT'S CATALOG NUMBER
4. TITLE (and Subtitle): (6) LARGE AMPLITUDE IRREGULARITIES AT LOW LATITUDES IN THE TOPSIDE IONOSPHERE.	5. TYPE OF REPORT & PERIOD COVERED: Scientific. Interim.
	6. PERFORMING ORG. REPORT NUMBER: ERP, No. 616
7. AUTHOR(s): (10) W.J. Burke* M.C. Kelley** D.E. Donatelli* R.C. Sagalyn	8. CONTRACT OR GRANT NUMBER(s): (16) 2311 (17) G2
9. PERFORMING ORGANIZATION NAME AND ADDRESS: Air Force Geophysics Laboratory (PHR) Hanscom AFB, Massachusetts 01731	10. PROGRAM ELEMENT, PROJECT, TASK AREA & WORK UNIT NUMBERS: 61102F 2311G205
11. CONTROLLING OFFICE NAME AND ADDRESS: Air Force Geophysics Laboratory (PHR) Hanscom AFB, Massachusetts 01731	12. REPORT DATE: (11) 28 Nov 1977
	13. NUMBER OF PAGES: 23 (12) 22p.
14. MONITORING AGENCY NAME & ADDRESS (if different from Controlling Office)	15. SECURITY CLASS. (of this report): Unclassified
	15a. DECLASSIFICATION/DOWNGRADING SCHEDULE

16. DISTRIBUTION STATEMENT (of this Report)

Approved for public release; distribution unlimited.

17. DISTRIBUTION STATEMENT (of the abstract entered in Block 20, if different from Report)

18. SUPPLEMENTARY NOTES

*Regis College Research Center, Weston, Massachusetts 02193
**Cornell University, Ithaca, New York 14853

19. KEY WORDS (Continue on reverse side if necessary and identify by block number)

Ionosphere irregularities
Topside irregularities
Equatorial spread F

20. ABSTRACT (Continue on reverse side if necessary and identify by block number)

Observations from the high resolution spherical electrostatic analyzer experiment aboard ISIS I have been used to study large amplitude irregularities at low latitudes in the topside ionosphere. The irregularities appeared as plasma depletions near the magnetic equator and were observed up to satellite apogee (3500 km). The altitude-local time distribution of the depletions was such that those at altitudes greater than 2000 km were found only in the post-midnight sector. This result agrees with the predictions of a simple MHD model for plasma bubbles drifting under the influence of gravity-buoyancy forces.

DD FORM 1 JAN 73 1473 EDITION OF 1 NOV 65 IS OBSOLETE

Unclassified
SECURITY CLASSIFICATION OF THIS PAGE (When Data Entered)

409 578 JOB

Preface

We wish to thank W. P. Sullivan of AFGL for his role in the development of the electrostatic analyzer experiment aboard ISIS I. This work was supported in part by Air Force Contract Numbers F19628-75-C-0081 and F19628-77-C-0122.

Contents

1.	INTRODUCTION	7
2.	THE EXPERIMENT	8
3.	THEORETICAL CONSIDERATIONS	9
	3.1 The Woodman-LaHoz Model of Plasma Bubbles	9
	3.1.1 MHD Stability of Bubbles	9
	3.1.2 Drift Motions of Bubbles	10
4.	OBSERVATIONS	12
	4.1 Selection Criteria	12
	4.2 Longitude-Latitude Distribution	12
	4.3 Examples of ISIS Data	14
5.	DISCUSSION	16
6.	SUMMARY AND CONCLUSIONS	18
REFERENCES		21
APPENDIX A:	Stability of Bubbles Against Drift Wave Induced Diffusive Collapse	23

Illustrations

1. Cross Section of Magnetically Aligned, Cylindrical Plasma Bubble of Radius a 9
2. The Geographic Longitude and Latitude Distribution of Orbits Along Which Large Amplitude Irregularities (dark portions of lines) Were Observed 13
3. Ion Densities as Functions of Altitude and Geographic Latitude for Orbits #242 and #253 13
4. Ion Densities as Functions of Altitude and Geographic Latitude for Orbits #218 and #219 14
5. Ion Densities as Functions of Altitude and Geographic Latitude for Orbits #3194 and #3530 14
6. Scatter Plot of the Latitudes at Which Plasma Depletions Were Observed as a Function of Local Time 18

Large Amplitude Irregularities at Low Latitudes in the Topside Ionosphere

1. INTRODUCTION

The recent theoretical analyses[1,2,3] of equatorial spread F phenomena have been spurred by observations from incoherent radar backscatter[4,5] and from satellite[6,7] and rocket-borne instruments.[8] Spread F appears after sunset as a magnetically aligned depletion of plasma in the bottom- or top-side of the equatorial F region. The present consensus is that the depletions result from a Rayleigh-Taylor instability[2,8] generated at the sharp plasma density gradient of the post-sunset bottomside F layer. According to this theory, depletions can propagate to, or slightly higher than, the peak of the F region. Numerical calculations[9] and McDonald et al[10] have shown that in the non-linear evolution of the collisional Rayleigh-Taylor instability the plasma depletions percolate like bubbles beyond the F layer peak. The drift motions of fully evolved plasma bubbles have been studied by Ott.[11]

Observations from satellite-borne instruments have shown large "bite outs" of plasma as satellites passed through regions of spread F. Decreases in plasma density of up to two to three orders of magnitude were measured by means of instruments on OGO 6 (Hanson and Santani)[12] at altitudes near 400 km. These plasma decreases were coincident with enhanced fluxes of heavy ions. Woodman and

(Received for publication 28 November 1977)

(Because of the large number of references cited above, they will not be listed here. See Reference Page 21 for References 1 through 12.)

LaHoz[5] interpreted the enhanced flux of heavy ions as indicating that the depletions originated at altitudes below 400 km. Recent observations from the drift meter experiment on Atmospheric Explorer C at similar altitudes tend to confirm this suggestion. McClure et al[7] found that, generally, the plasma within the depletions was moving vertically with speeds of ~150 m/sec and, in the ambient plasma's rest frame of reference, to the west at lesser speeds. These measured drift speeds were an order of magnitude larger than those calculated by Scannapieco and Ossakow.[9]

Here we report on large amplitude irregularities observed in the equatorial topside ionosphere by means of a spherical electrostatic analyzer (SEA) aboard ISIS I. The instrumentation is described briefly in Section 2. To help interpret the observations, we investigate the magnetohydrodynamic (MHD) properties of plasma bubbles in the topside ionosphere, as suggested by Woodman and LaHoz.[5] Examples of the depletions are presented to illustrate their day to day, orbit to orbit, and altitude variability. In Section 5 we consider the altitude-local time distribution of topside plasma depletions. It is shown that depletions at altitudes > 2000 km only appear in the post-midnight sector. The high altitude observations are consistent with a model of plasma bubbles formed near 300 km and floating with mean vertical speeds of ~130 m/sec.

2. THE EXPERIMENT

ISIS I was launched into polar orbit on 30 January 1969 with an apogee of 3526 km, a perigee of 525 km, and an inclination of 88.4°. The SEA, which is mounted on a 96-cm boom, consists of a solid collector (1.9-cm radius) surrounded by two wire-mesh grids (2.54- and 3.18-cm radii). It is electrically designed to measure the thermal ion density, the ion energy distribution between 0 and 50 eV, the satellite potential, and the ratio of ion mass to temperature. The reduction of probe data is based on the motion of charged particles in a central force field.[13, 14, 15] Data presented in this report were measured while the instrument was in the ion density mode of operation. The range of sensitivity of the SEA is 10 - 10^6 cm^{-3} while the satellite is in darkness. Due to photoelectron emission from the collector, when the satellite is in sunlight the lower limit is 700 cm^{-3}. The sampling rate is 60 per sec and corresponds to a spatial resolution of 150 m.

13. Sagalyn, R.C., Smiddy, M., and Wisnia, J. (1963) Measurement and interpretation of ion density distributions in the daytime F region, J. Geophys. Res. 68:199.

14. Smiddy, M., and Stuart, R.D. (1969) An Analysis of the Behavior of a Multigrid Spherical Sensor in a Drifting Maxwellian Plasma, AFCRL-69-0013.

15. Whitteker, J.H., Brace, L.H., Burrows, J.R., Hartz, T.R., Heikkila, W.J., Sagalyn, R.C., and Thomas, D.M. (1972) ISIS I observations of the high latitude ionosphere during a geomagnetic storm, J. Geophys. Res. 77:6121.

3. THEORETICAL CONSIDERATIONS

3.1 The Woodman-LaHoz Model of Plasma Bubbles

Before proceeding to ISIS data, it is useful to expand upon the suggestion of Woodman and LaHoz[5] that in the topside ionosphere spread F depletions act as bubbles of plasma that convect in a manner determined by buoyancy forces. Since all of the data were measured in the topside ionosphere, this procedure provides a standard with which the observations can be easily compared.

Let us consider the magnetohydrodynamic (MHD) properties of a plasma bubble formed in the bottomside ionosphere that has convected to the peak of the F layer. For simplicity assume that the bubble is a cylinder of length L and a radius a, where L >> a. A set of coordinates is chosen with x, y, and z positive toward the west, vertical, and north, respectively (Figure 1). The magnetic and gravitational fields are in the +z and -y directions respectively. We ask two questions: Is such a bubble stable against MHD collapse? and In what direction will the bubble drift?

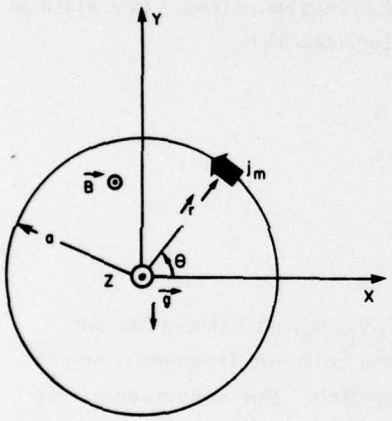

Figure 1. Cross Section of Magnetically Aligned, Cylindrical Plasma Bubble of Radius a. The coordinate axes X, Y, and Z are positive toward the west, vertical, and north, respectively. The particle pressure for $r < a$ is significantly less than that outside the bubble. The pressure gradient is supported by magnetization currents (j_m) flowing in the direction $+\theta$ increasing along the bubble's surface

3.1.1 MHD STABILITY OF BUBBLES

In considering the stability of the bubble, we ignore the effects of gravity and write the pressure balance equation

$$p(r) + \frac{B^2(r)}{8\pi} = \text{const} ,$$

where p(r) and B(r) are the particle pressure and the magnetic field at a distance r from the central axis of the bubble. The particle pressure has a local minimum and the magnetic field a local maximum inside the bubble. The intensified magnetic

field within the bubble results from magnetization currents [$j_m(r)$] flowing in the $+\theta$ direction (Figure 1) along the bubble surface. The magnitude of the current is

$$j_m(r) = \frac{1}{B(r)} \frac{dp(r)}{dr} .$$

The $\vec{j}_m \times \vec{B}$ force is directed radially out from the bubble surface.

The stability of the bubble may be tested by applying the Rosenbluth criterion.[16] If a portion of the surface is displaced inward, then the $\vec{j}_m \times \vec{B}$ force in the vicinity of the displacement increases. Because this force is in the opposite direction to the displacement, the increased $\vec{j}_m \times \vec{B}$ force tends to restore the bubble's surface to its original configuration. In this sense, the bubble is a stable configuration not subject to catastrophic MHD collapse. The bubble's stability against slow collapse due to cross-field line diffusion arising from unstable drift waves at the bubble's surface is discussed below and in Appendix A.

3.1.2 DRIFT MOTIONS OF BUBBLES

The drift motions of plasma bubbles are specified by the forces acting on the particles, subject to the constraint that currents be divergence-free. In a state of equilibrium, the equations of motion for ions and electrons are

$$-\nabla p_i + ne\left(\vec{E} + \frac{\vec{v}_i}{c} \times \vec{B}\right) + nm_i\vec{g} - m_i n\nu\left(\vec{v}_i - \vec{U}\right) = 0$$

and

$$-\nabla p_e - n_e\left(\vec{E} + \frac{\vec{v}_e}{c} \times \vec{B}\right) = 0 ,$$

where p_i and p_e are the ion and electron pressures; v_i, v_e, and U are the ion, electron, and neutral velocities; ν is the ion-neutral collision frequency; and $\vec{E}$ and $\vec{g}$ are the electric field and gravitational acceleration. For convenience, we adopt the coordinates specified in Figure 1, and assume that B = constant and that no physical quantity varies with z. Following Ott,[11] we define an effective gravitational acceleration $\vec{g}' = \vec{g} + \vec{\nu u}$. This effective gravity causes a current to flow in the $(\vec{g}' \times \hat{z})$ direction. In the region of lower density this current would be smaller, unless an electric field built up to drive a Pederson current. The continuity of current equation gives

$$\frac{ncm_i(\vec{g}' \times \hat{z})}{B} = \sigma_p^* \vec{E} + \frac{\overset{*}{n}cm_i(\vec{g}' \times \hat{z})}{B} ,$$

16. Chandraseklar, S. (1960) Plasma Physics, Phoenix Books, Univ. of Chicago Press, Chicago, Illinois, p. 101.

where n and n^* are the plasma densities outside and inside the bubble, respectively, $\sigma_p{}^* = (n^* ecv/B\Omega_i)$ is the Pedersen conductivity inside the bubble, Ω_i is the ion cyclotron frequency. The polarization electric field inside the bubble is

$$\vec{E} = \frac{n - n^*}{n^*} \frac{m_i(\vec{g}' \times \hat{z})}{(e\nu/\Omega)} .$$

This electric field in turn leads to a drift motion of the bubble relative to the ambient plasma:

$$\vec{V}_B = -\frac{n - n^*}{n^*} \frac{\vec{g}'}{\nu} .$$

In the post-sunset F region, neutral winds are predominantly eastward ($-\hat{x}$ direction); thus, the bubble's drift velocity,

$$\frac{n - n^*}{n^*} \frac{g}{\nu} \hat{y} + U \hat{x} ,$$

is vertically up and to the west relative to the ambient plasma. We note that the ambient plasma may be superrotating.[17,18] In this case the bubble's drift might appear to be eastward to an observer in the corotating frame of reference.

At altitudes where ion-neutral collisions are unimportant, the effects of neutral winds vanish so that both the bubble and the ambient plasma corrolate with the earth. Also, current continuity cannot be maintained via Pederson currents in a collisionless plasma. The $\vec{g} \times \vec{B}$ should continue to pile up charge ($\nabla \cdot \vec{j} = \partial\rho/\partial t$) and the electric field would increase with time. Thus, the bubble would be accelerated upwards. Ott[11] was able to show that in the collisionless case the equations were the same as those for an ideal fluid. In this case the upward acceleration is balanced by a drag due to the generation of vortices in the ambient plasma. Plasma vortices carry away the excess charges that are accelerating the bubble. In the steady state, vortices are shed at the same rate that charge is piled up. The bubble would approach a terminal velocity that is proportional to (n - n*) and to the square root of the bubble's radius.

This model has implications as to the local times at which the bubbles may be observed if they have sufficient stability and buoyancy to drift to altitudes greater than 1000 km. For example, a bubble that is formed at 2100 LT and 300 km with a mean vertical drift of 150 m/sec and a westward drift of 100 m/sec relative to the ambient plasma would reach an altitude of 2000 km at 2330 LT and 3000 km at

17. Rishbeth, H. (1971) Polarization fields produced by winds in the equatorial F-region, Planet. Sp. Sci. 19:357.

18. Woodman, R. F. (1972) East-west ionospheric drifts at the magnetic equator, Space Res. 12:969.

0100 LT. The calculations assume that the ambient plasma is corotating. The bubbles would reach these altitudes at later local times if the ambient plasma is superrotating. Thus, it would be impossible to observe plasma bubbles at altitudes greater than 2000 km in the early evening local time sector.

4. OBSERVATIONS

4.1 Selection Criteria

All data collected during ISIS I's first year of operation were examined to identify periods when the satellite was in the 2000 to 0300 local time sector and between 45°N and 45°S geographic latitude. Data were selected for further analysis only if measurements were made up to the magnetic equator. Only about three hundred orbits fulfilled these requirements. Large amplitude irregularities were observed during 21 of these orbits. The irregularities were considered to be of large amplitude only if the peak to trough density ratio was 2 or greater.

4.2 Longitude-Latitude Distribution

The geographical longitude and latitude distribution of orbits during which large amplitude irregularities were observed is given in Figure 2. Solid lines denote the sampling extent of each pass, with the heavier portion indicating the region of observed irregularities. The dashed line gives the location of the magnetic equator. The irregularities were confined to within ± 15° of the magnetic equator, with nearly half having latitudinal extents greater than 10°. We note that 81 percent of the irregularities were observed between + and - 60° longitude. This geographic region was found by Basu et al[19] to have the highest percentage of scintillations during November - December 1969, 1970.[19] To illustrate the ISIS I observations in the topside ionosphere, we have chosen four pairs of orbits for presentation (Figures 3, 4, and 5). These figures show: the day to day variability at a given altitude, longitude, and local time; the orbit to orbit variability at a given altitude and local time; and ion density depletions at altitudes > 1500 km, respectively.

19. Basu, S., Basu, S., and Khan, B.K. (1976) Model of equatorial scintillations from in situ measurements, Radio Sci. 11:821.

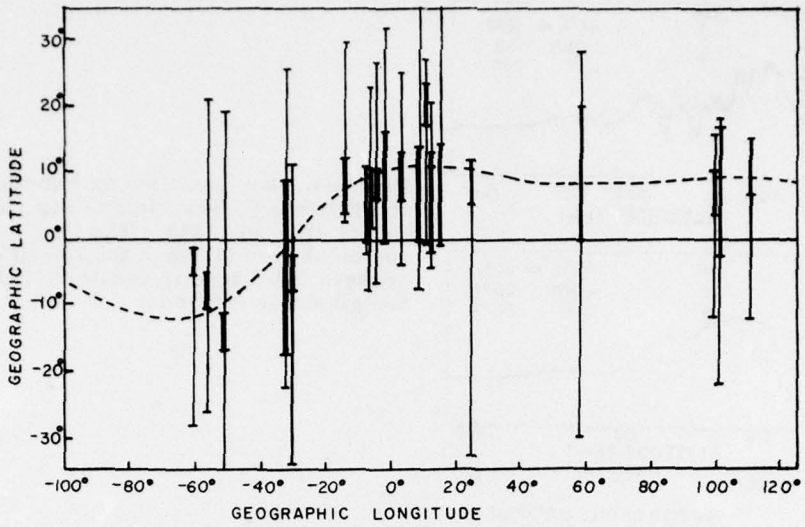

Figure 2. The Geographic Longitude and Latitude Distribution of Orbits Along Which Large Amplitude Irregularities (dark portion of lines) Were Observed. The dashed line represents the magnetic equator

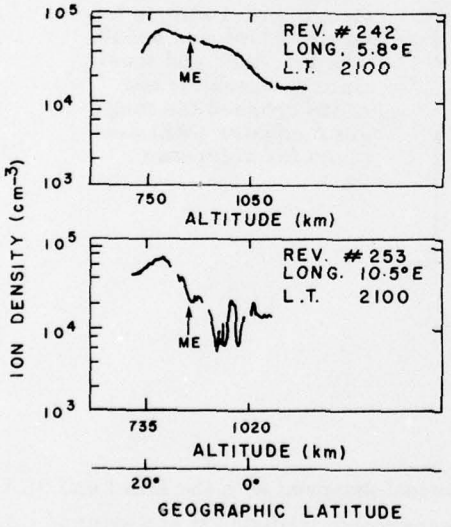

Figure 3. Ion Densities as Functions of Altitude and Geographic Latitude for Orbits #242 and #253. The longitude and local time at which the satellite crossed the magnetic equator (ME) are given for reference

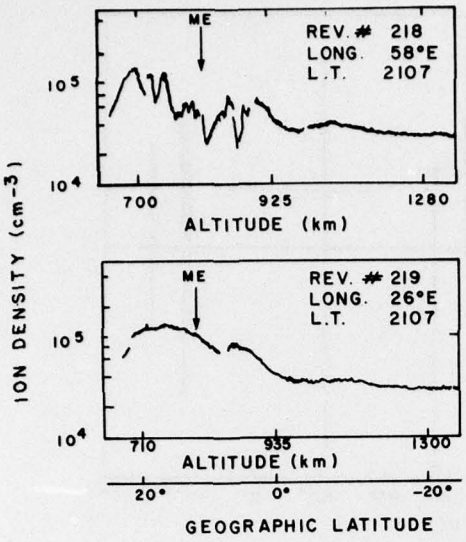

Figure 4. Ion Densities as Functions of Altitude and Geographic Latitude for Orbits #218 and #219. The longitude and local time at which the satellite crossed the magnetic equator (ME) are given for reference

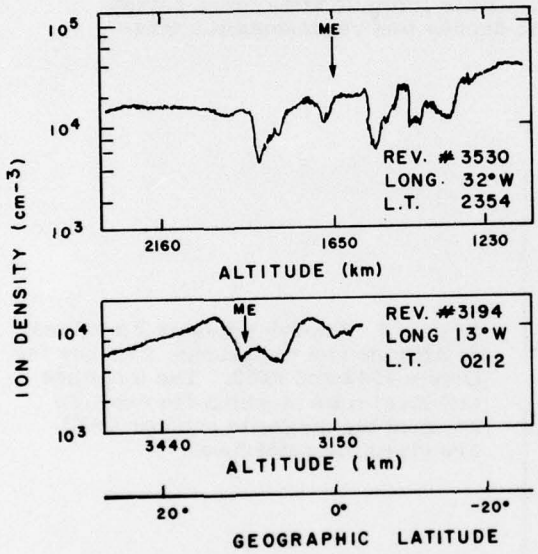

Figure 5. Ion Densities as Functions of Altitude and Geographic Latitude for Orbits #3194 and #3530. The longitude and local time at which the satellite crossed the magnetic equator (ME) are given for reference

4.3 Examples of ISIS Data

In Figure 3 we have plotted the ion densities observed with the ISIS I and SEA during orbits #242 and #253 as functions of geographic latitude (λ) and altitude (h). The longitude and local time at which the satellite crossed the magnetic equator (ME) are given for reference. This example illustrates the day to day variability found at a given longitude and local time. During orbits #242 and #253, the

satellite crossed the equator at longitudes 5.8°E and 10.5°E at a local time of 2100 and universal times of 2027 and 2054 on 20 and 21 February 1969, respectively. A maximum density of 8×10^4 cm^{-3} was observed at $\lambda = 17°$ and h = 775 km of #242. The density decreased slowly to 4×10^4 cm^{-3} at 2.5° (970 km) then moved quickly to a stable value of $\sim 1.5 \times 10^4$ at -4° (1070 km). During orbit #253, the maximum density was 7.1×10^4 cm^{-3} at 17° (790 km) then declined gradually, albeit in an irregular fashion, to 3×10^4 cm^{-3} at 7° (930 km). Two plasma "bite-outs" were measured at positions near 4.5° (970 km) and 1.5° (1015 km) where the density decreased to 6×10^3 and 4×10^3 cm^{-3}, respectively. If we assume that the density measured at these latitudes during orbit #242 represents the unperturbed ionosphere, then the decrease in both instances is by a factor of ~8. If the depletion amplitude is measured relative to the density immediately outside the "bite-out", then the decrease is by a factor of ~5.

The ion densities measured during orbits #218 and #219 (Figure 4) provide an example of orbit to orbit variability. In both instances the peak density was $\sim 1.5 \times 10^5$ cm^{-3} near $\lambda = 20°$ and h = 700 km. But where large amplitude irregularities were observed for about 8° on either side of the magnetic equator during #218, only a factor of ~2 depletion is observed near $\lambda = 8°$ during #219. In the case of #218, the density in the depleted region was $\sim 2 \times 10^4$, a factor of ~4 relative to the surrounding plasma.

Large amplitude irregularities were observed at low latitudes and at altitudes > 1500 km during six ISIS I orbits. Two examples from orbits #3530 and #3194 are given in Figure 5, where we have plotted ion densities as functions of altitude and geographic latitude. In the case of #3530, the irregularities were observed to extend from 9°N to 16°S and from 1800 to 1300 km. At $\lambda = 9°$ the ion density decreased abruptly from 1.5×10^4 to 4.5×10^3 cn^{-3}. After recovery near the equator, similar depletions were found centered near -5° and -12°. The large altitude range of the disturbance indicates that in this instance ISIS went through a series of plasma bubbles at different altitudes but at approximately the same magnetic longitude. This is consistent with numerical calculations by McDonald et al[10] showing that in the topside ionosphere the irregularities drift like a column of percolating bubbles. During the data collecting segment of #3194, the satellite was at altitudes greater than 3000 km. At $\Lambda = 10°$ the density decreased from 10^4 to 4×10^3 cm^{-3} before recovering to 1.1×10^4 cm^{-3} at $\Lambda = 20°$. In all instances the high altitude irregularities were well centered on the magnetic equator.

The examples of plasma depletions in Figures 3, 4, and 5 are quite representative of those observed during the entire 21 orbits. In 13 of the 15 orbits during which depletions were observed below 1500 km, the minimum density within the depletions ranges between 2 and 5×10^4 cm^{-3}. In the cases of #253 (Figure 3) and #3686 as well as the six orbits at altitudes above 1500 km, the minimum density in

the depletions was < 10^4 cm^{-3}. The depletion amplitudes, which we define as the ratio for the density outside to the minimum density inside a depletion region, ranged between 2 and 8.

5. DISCUSSION

In the previous section we presented ISIS I observations of low-latitude, large-amplitude irregularities in the topside ionosphere. Here we discuss their relationship to other in situ measurements and some implications for understanding equatorial ionospheric processes. This is done by considering the ion densities measured within depletions and their altitude-local time distribution. Figures 2 and 3 of Hanson and Santani[12] provide examples of plasma decreases from ~10^6 to 1 - 2 × 10^3 cm^{-3} at 400 km near the magnetic equator. Similar examples are found in data from Atmospheric Explorer-C (McClure et al).[7] The "typical" equatorial observations from OGO-6 given in Figures 2 and 4 of Basu et al[19] show much less severe depletions. There were 15 ISIS I orbits along which plasma depletions were observed at altitudes less than 1500 km. Only during two of these orbits (#253 and #3686) did the density within the depletion become less than 10^4 cm^{-3}. In the other examples, the minimum density within the depletion ranges between 2 and 6 × 10^4 cm^{-3}. The minimum density observed within depletions at altitudes > 1500 km ranged between 1 and 5 × 10^{-3}. This is consistent with the plasma bubble model of Woodman and LaHoz.[5] The net gravity-buoyancy force is vertically up only where the density within the irregularity is less than that of the surrounding ionosphere.

The plasma bubbles observed by means of ISIS I in the topside of the F region are fully evolved density depletions. Thus, the non-linear theories of Scannapicco and Ossakow[9] and Ott[11] are most relevant. The former is a computer simulation that shows that an initial perturbation on the bottomside of the F peak pinches off due to recombination and rises into the topside. Where ion-neutral collisions are important, the bubble drifts up and to the west under the influence of gravity and neutral wind-induced electric fields. This is essentially the same argument given by Woodman and LaHoz[5] to explain the observed tilt of plumes at Jicamarca. In the collisionless topside region the bubbles continue to rise, reaching a terminal velocity that is proportional to (n - n*) and to the square root of the bubble's radius (Ott)[11]. This non-linear model predicts that only large plasma bubbles are able to reach very high altitudes. The typical terminal velocity of ~100 m/sec calculated by Ott is consistent with the ISIS I observations of plasma depletions above 2000 km in the post-midnight sector.

Previously we have shown that in the topside ionosphere plasma bubbles are stable against catastrophic MHD collapse. However, diffusive processes may lead to collapse of the bubbles before they reach their floatation level. Woodman and Basu[20] have shown that the equatorial irregularity spectrum frequently is non-monotonic at wavelengths near the ion gyroradius.

Kelley[21] suggested that the non-monotonic feature of the spectrum is due to unstable drift waves driven by sharp density gradients on the surface of the irregularities. Kadomtsev[22] has shown that unstable drift waves produce cross field line diffusion at rates approaching the Bohm limit. A dimensional analysis of the diffusion equation, given in Appendix A, indicates that some plasma bubbles with radii of a few tens of kilometers are sufficiently long-lived to reach altitudes > 2000 km.

Figure 6 is a scatter plot of the altitudinal extent of low-latitude plasma depletions as a function of local time. The altitude–local time sectors from which we have no low-latitude observations are designated by slanted lines. During the May-July 1969 period ISIS I was near apogee at low-latitudes in the midnight-evening sector (marked by dots). In this period 228 orbits met the selection criteria. However, there were no instances of plasma depletions, indicating that they are excluded from this altitude–local time sector. The plasma depletions observed between 1200 km and satellite perigee tended to cluster in the 2000 to 2200 local time sector. Those detected at altitudes > 2000 km were in the post-midnight sector. This altitude-local time distribution indicates that the plasma depletions observed by ISIS I originated at low altitudes near local sunset.

For example, if we assume that the depletion observed during orbit #3194 (Figure 5) originated at ~300 km and 2000 LT, then its mean vertical drift velocity was ~130 m/sec. Although this is consistent with the in situ measurements of McClure at al,[7] care must be exercised in generalizing the model for where depletions may be detected. There is one example of a plasma depletion at 2215 LT and ~600 km (Figure 6). Observations from OGO-6 (Basu et al,[19] Figure 2) and Atmospheric Explorer-C (McClure et al[7]) at altitudes < 600 km indicate the existence of plasma bite-outs near local midnight. Thus, the conditions for the onset of spread F are not restricted to the immediate post-sunset local time sector. The model for the topside drifts of plasma bubbles would indicate that depletions should be detectable throughout the unexplored altitude-local time sector in the lower left portion of Figure 6.

---

20. Woodman, R. F., and Basu, S. (1977) Comparison between in situ spectral measurements of equatorial spread F region irregularities and backscatter observations at 3m wavelength, Trans. Amer. Geophys. U. 58:449.

21. Kelley, M. C. (1977) Plasma turbulence in the equatorial F region ionosphere, Trans. Amer. Geophys. U. 58:473.

22. Kadomtsev, B. B. (1965) Plasma Turbulence, Academic Press, New York.

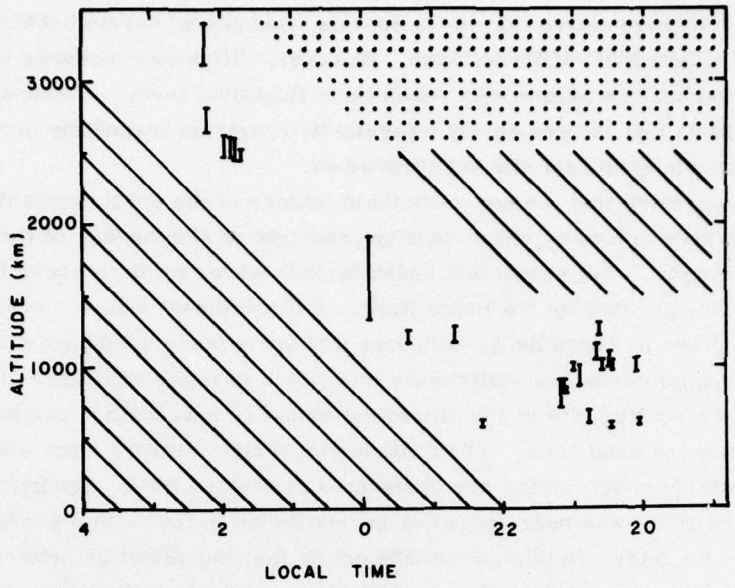

Figure 6. Scatter Plot of the Latitudes at Which Plasma Depletions Were Observed as a Function of Local Time. The regions of no observations are indicated by slanted lines. In the region marked by dots, there were over 200 orbits that crossed the magnetic equator, but no observed depletions

6. SUMMARY AND CONCLUSIONS

In this report we have presented observations of large-amplitude irregularities at low-latitudes in the topside ionosphere from the electrostatic analyzer experiment aboard ISIS I. Data from the satellite's first year of operation show 21 examples of plasma depletions at night, near the magnetic equator in the altitude range $600 \leq h \leq 3500$ km. Eighty-one percent of the depletions were found in the $\pm 60°$ longitude sector, the region of most frequent ionospheric scintillations (Basu et al[19]). The minimum depletions found within the depletions ranged from 2×10^3 to 6×10^4 cm^{-3}. The lowest densities were observed in depletions at altitudes greater than 1500 km. The depletion amplitudes ranged from 2 to 8. Though these are considerably less than the 2 to 3 orders of magnitude depletion reported by Hanson and Santani[12] at lower altitudes, they are not inconsistent with OGO-6 results. In one instance (#3430, Figure 5), the satellite passed through a series of plasma bubbles between 1800 and 1300 km. This observation is consistent with recently presented numerical calculation by McDonald et al.[10]

To help understand our observations of plasma depletions in the topside ionosphere, we have developed a simple MHD bubble model along lines suggested by Woodman and LaHoz.[5] In agreement with results from Atmospheric Explorer-C, the model predicts that the bubbles should drift vertically up and, in the rest frame of the ambient plasma, to the west. It also predicts that bubbles reaching altitudes greater than 2000 km should appear only in the post-midnight sector. The ISIS I observations agree with this prediction.

References

1. Haerendel, G. (1974) Theory of Equatorial Spread F, Max Plank Institut für Physik und Astrophysik.
2. Balsley, B.B., Haerendel, G., and Greenwald, R.A. (1972) Equatroial spread F: recent observations and a new interpretation, J. Geophys. Res. 77:5625.
3. Hudson, M.K., and Kennel, C.F. (1975) Linear theory of equatorial spread F, J. Geophys. Res. 80:4581.
4. Farley, D.T., Balsley, B.B., Woodman, R.F., and McClure, J.P. (1970) Equatorial spread F: implications of VHF radar observation, J. Geophys. Res. 75:7199.
5. Woodman, R.F., and LaHoz, C. (1976) Radar observations of F region equatorial irregularities, J. Geophys. Res. 81:5447.
6. Hanson, W.B., and Santani, S. (1971) Relationship between F_e^+ ions and equatorial spread F, J. Geophys. Res. 76:7761.
7. McClure, J.P., Hanson, W.B., and Hoffman, J.F. (1977) Plasma bubbles and irregularities in the equatorial Ionosphere, J. Geophys. Res. 82:2650.
8. Kelley, M.C., Haerendel, G., Kappler, H., Valenzuela, A., Balsley, B.B., Carter, D.A., Ecklund, W.L., Carlson, C.W., Hauser, B., and Torbert, R. (1976) Evidence for a Rayleigh-Taylor type instability and upwelling of depleted density regions during equatorial spread F. Geophys. Res. Lett. 3:448.
9. Scannapieco, A.J., and Ossakow, F.L. (1976) Nonlinear equatorial spread F, Geophys. Res. Lett. 3:451.
10. McDonald, B.E., Ossakow, S.L., and Zalesak, S.T. (1977) Multiple equatorial F region plasma depletions, Trans. Amer. Geophys. U. 58:455.
11. Ott, E. (1977) Theory of Rayleigh-Taylor Bubbles in the Equatorial Ionosphere, Cornell University, preprint.
12. Hanson, W.B., and Santani, S. (1973) Large N_i gradients below the equatorial F Peak, J. Geophys. Res. 78:1167.

13. Sagalyn, R.C., Smiddy, M., and Wisnia, J. (1963) Measurement and interpretation of ion density distributions in the daytime F region, J. Geophys. Res. 68:199.

14. Smiddy, M., and Stuart, R. D. (1969) An Analysis of the Behavior of a Multigrid Spherical Sensor in a Drifting Maxwellian Plasma, AFCRL-69-0013.

15. Whitteker, J.H., Brace, L.H., Burrows, J.R., Hartz, T.R., Heikkila, W.J., Sagalyn, R.C., and Thomas, D.M. (1972) ISIS I observations of the high latitude ionosphere during a geomagnetic storm, J. Geophys. Res. 77:6121.

16. Chandraseklar, S. (1960) Plasma Physics, Phoenix Books, Univ. of Chicago Press, Chicago, Illinois, p. 101.

17. Rishbeth, H. (1971) Polarization fields produced by winds in the equatorial F-region, Planet. Sp. Sci. 19:357.

18. Woodman, R.F. (1972) East-west ionospheric drifts at the magnetic equator, Space Res. 12:969.

19. Basu, S., Basu, S., and Khan, B.K. (1976) Model of equatorial scintillations from in situ measurements, Radio Sci. 11:821.

20. Woodman, R.F., and Basu, S. (1977) Comparison between in situ spectral measurements of equatorial spread F region irregularities and backscatter observations at 3m wavelength, Trans. Amer. Geophys. U. 58:449.

21. Kelley, M.C. (1977) Plasma turbulence in the equatorial F region ionosphere, Trans. Amer. Geophys. U. 58:473.

22. Kadomtsev, B.B. (1965) Plasma Turbulence, Academic Press, New York.

Appendix A

Stability of Bubbles Against Drift Wave Induced Diffusive Collapse

In Section 3 of this report we made use of the Rosenbluth criterion[16] to show that in the ionosphere plasma bubbles are stable against catastrophic MHD collapse. However, due to finite Larmour radius effects, the magnetization currents responsible for the bubbles MHD stability also give rise to unstable drift waves. Drift waves with wavelengths near the ion gyroradius (ρ_i) are efficient sources of cross field line diffusion (Kadomtsev).[22] The diffusion coefficient can approach the Bohm diffusion limit

$$D_B = \rho_i v_i$$

where v_i is the ion thermal velocity. It is possible to calculate a lower bound on the lifetime of a plasma bubble against drift-wave-induced diffusive collapse. We assume that the diffusion proceeds at the Bohm limit. The approximate lifetime of such a bubble is

$$T_B = a^2 / D_B$$

where a is the radius of the bubble (Figure 1). If B = 0.25 gauss and 0^+, the dominant ion, has a temperature of 1000°, then $D_B = 6.9 \times 10^7$ cm^2 sec^{-1}. A bubble with a radius of 50 km has a lifetime of about 100 hours. Since this is much greater than the 1 to 7 hours after birth in which ISIS I may observe bubbles, they may be considered stable against diffusive collapse.